Nanostuctures of gold and TiO$_2$, CeO$_2$ and CuO supported on inert surface: controlled formation of the active interface and its catalytic properties

1. Introduction and outline of the research work reported here

Metal nanoparticles constitute a bridge between molecular and metallic states and possess specific physical, chemical and catalytic properties. However, due to the high surface excess energy nanosize metals are very sensitive and in the absence of sufficient stabilization thermo dynamical driving forces cause their aggregation.

Since Haruta discovered the surprisingly high catalytic activity of nanosize gold, tremendous work has been done in the field of Au catalysis[1]. Small Au particles with large specific surface area can be prepared by different methods; one of them is the highly promising colloid chemical route. In this case reduction of HAuCl$_4$ precursor in water produces Au sol, in which several nm size Au particles are able to maintain their integrity only in the presence of stabilizers. The next deposition step which is required if heterogeneous catalyst is aimed to be produced is a key point To obtain homogeneous distribution of Au, the preformed metal particles of sol must be adsorbed onto solid oxide support by providing sufficient strong interaction between the stabilized particles and the surface of oxide. Stabilizers, however, must be eliminated before catalytic run by calcination treatment.

Research studies on gold try to discover and expand the range of applicability of Au among others in selective oxidation reactions and explain the structure-activity relationship[2]. It is widely accepted that in the most studied CO oxidation the activity depends on the particle size[3] and oxidation state of Au and the type and structure of oxide support[4,5]. The oxide-metal interface plays a crucial role in the CO oxidation mechanism proposed[6]. CeO$_2$, TiO$_2$, Fe$_2$O$_3$, etc. are considered to be "active supports" since they provide good activity for Au, while SiO$_2$, Al$_2$O$_3$ or MgO can be regarded as inactive or much less active supports[7]. For inactive supports the oxygen adsorption was suggested to happen on the defect sites of Au that is why the activity shows stronger dependence on the dispersion. In the case of reducible active oxides able to act as oxygen reservoir the microstructure of oxide and the nature of metal-support interface are of key importance because oxygen activation is suggested to happen mainly there[8].

Extensive research focusing on the controlled formation of Au-oxide interface has been pursued in our laboratory. We have studied model systems of gold/iron oxide[9,10] or gold/titania interface on SiO$_2$/Si(100)[11] and powder catalysts, when Au nanoparticles are supported on TiO$_2$[12] or TiO$_2$-SiO$_2$[13] oxides.

When a bulk active oxide support is used to disperse gold nanoparticles, it is obvious that Au-oxide interface is created. A rather challenging task is to ensure the intimate contact of these two components when the active oxide is applied only as a modifier in such an amount that is comparable with the amount of Au and large surface area SiO$_2$ support is used only to prevent sintering and aggregation of metal. The commonly studied case, when the inert support is modified by active oxide (TiO$_2$, CeO$_2$, etc) *prior* to the introduction of gold, producing for example Au/TiO$_2$-SiO$_2$ system[14]. In contrast to this, when active oxide is introduced last to the preformed Au/SiO$_2$ or the "(active oxide +Au)" is put on the inert support at the same time, a so-called "inverse" system can be produced, when the surface of Au is decorated with active oxide moieties realizing the

approach we call "localized oxide promotion" of gold. In all cases new catalytic properties are expected to appear compared to the usual Au/bulk active oxide catalysts and so we can gain new insights into the mechanism of CO oxidation on gold.

In the present research project we investigated the effect of 3 types of active oxides, TiO_2, CeO_2 and CuO on the structure and catalytic behaviour of SiO_2-supported gold according to the above described approach. Our aim was to ensure the intimate contact of nanosize active oxide and gold on SiO_2 support. Using gold sols, titania/ceria/copper oxide coverage on and around Au nanoparticles was produced. The different catalytic activity of the SiO_2 supported samples, depending on the type and the loading of oxide pointed out the importance of organic stabilizers present during the preparation and governing the final catalyst structure by special interactions with the oxide precursors.

In the next sections the already published research areas will be briefly introduced; however, the results just submitted (see the attached manuscript submitted to J. Phys. Chem C) or close to submission (section 5) will be discussed in more details.

2. General preparation methods, main experimental techniques applied

Here only the common methods are mentioned which were applied during our research focused on the TiO_2, CeO_2 and CuO-modified Aerosil supported gold catalysts. There were a few special techniques or preparation routes not common for the 3 main topics of the work. These are introduced shortly in the actual section.

For the synthesis of catalysts the following materials were used: aqueous solutions of $HAuCl_4*3H_2O$, tannic acid, sodium-citrate, poly(diallyldimethylammonium) chloride (PDDA), Ti(IV) bis(ammoniumlactato)dihydroxide (TALH), cerium(III) nitrate hexahydrate, Cu(II) nitrate trihydrate, and ceria nanopowder, Aerosil 200 silica, Eurotitania, Degussa P25 TiO_2 supports.

Gold hydrosol with an average particle size of d_{Au}~6 nm was produced by reduction of $HAuCl_4$ with a mixture of tannic acid and sodium citrate at 60^oC in water. The red color of the sol evidenced the reduction of Au^{3+} ions.

The above sol was used as "parent sol" in the next steps, when the Ti, Ce or Cu components were introduced in two different ways. In preparation method A, calculated amount of precursors of oxide modifiers were added to the Au sols at room temperature, then the temperature was increased to 60^oC within 1 h and kept there for 4 hours. Then, the adsorption of Ti or Ce or Cu-containing Au sol (composite sol) was accomplished with the aid of PDDA onto Aerosil SiO_2. The solid was separated by filtration, washed thoroughly with water and dried. Au/SiO_2 references was prepared also by the sol adsorption method. The nominal Au content of all the samples was kept at ~2 wt%, and this value was ascertained in several samples.

In preparation method B, the Au/SiO_2 reference sample was further processed. The dried sample in aqueous suspension was mixed with the appropriate amount of the oxide precursor, then the temperature was raised to $60-65^oC$ and the water was allowed to evaporate (it took usually 4-5 hours).

The Aerosil supported samples prepared by method "A" are denoted by AMeX where the letter A means method A, Me refers to Ti, Ce or Cu modifier and the number that follows indicates the oxide modifier's content in wt%. The samples produced by method "B" are labeled in the same way but with starting letter B. For the sake of correct comparison, a "blank" TiO_2 or CuO-modified SiO_2 was prepared by method "B" on SiO_2 after PDDA preadsorption.

The Zeta potential of Au sol was determined by dynamic light scattering measurements using a Malvern Zeta Sizer apparatus to characterize the electrostatic interactions that may control the formation of supported samples.

Determination of metal content of the samples was done either by a double-focusing inductively coupled plasma mass spectrometer (ICP-MS) or by radioisotope induced X-ray fluorescence spectrometry (XRF) method.

The phase composition of crystalline components of selected samples was investigated by X-ray diffraction (XRD). The crystallite size for each phase was determined from the full width at half maximum of the first peak using the Scherrer-equation.

Reducibility of Cu-containing samples was investigated with temperature programmed reduction technique (TPR) of precalcined samples using 5% H_2 in He.

The distribution and the size of Au and the modifier oxides were studied by a conventional transmission electron microscope (TEM) equipped with energy dispersive spectrometer (EDS) for electron probe microanalysis. High resolution transmission electron microscope (HRTEM) investigations were carried out, when the visualisation of lattice fringes were required.

CO oxidation was measured at atmospheric pressure in a plug flow reactor connected to a QMS. Temperature programmed reaction was performed with a gas flow of 0.54% CO + 9.1 % O_2 in He (CO/O_2=1/18) or in the case of CuO-modified samples (section 5) in 1% O_2 + 1% CO in He (CO/O_2=1) as well, with different flow rates and amounts of catalyst. Preferential oxidation of CO in the presence of hydrogen (PROX) was carried out first with 1% CO + 1% O_2 + 62% H_2 in He with QMS and GC analysis (TiO_2- and CeO_2-modifications), later on with 1% CO + 1% O_2 + 60% H_2 in He with QMS analysis (CuO-modifications) with different flow rates and amounts of catalyst.

3. Investigation of the Au-TiO$_2$/SiO$_2$ systems[14]

In the literature a few studies could be found on core-shell structured nanoparticles made of titania core and gold shell[15,16]. These composite particles were prepared to study optical properties or photocatalytic activity[17, 18]. Philip et al.[19,20] published a one step synthesis of Au core/TiO_2 or ZrO_2 shell particles from $HAuCl_4$ and titanium isopropoxide or zirconium propoxide under reflux. The TiO_2 shell was suggested to form around the 50 nm sized Au particles, however, no TEM pictures were shown to verify that and only the optical properties of Au core/ZrO_2 shell composite were discussed in details. It seems that the application of Au/TiO_2 core-shell or layered structures in CO oxidation was hardly studied when the research work started 5 years ago.

3.1. Formation of Au-TiO$_2$ nanostructures on silica support

The gold sol preparation gave nicely reproducible particle size with $d_{Au}\sim6$ nm. It was also ascertained that the sol adsorption step onto the support did not change the original particle size. Table 1 shows the Au and Ti loading data and the Au particle size after calcination and catalytic tests determined by TEM.

Table 1 Metal loading and Au particle size after calcination and catalytic run

| sample	Au content (wt%)	TiO$_2$ content (wt%)	Ti/Au	d_{Au}^b (nm)
ATi0.2	2.0	0.2	0.2	
ATi0.8	1.8	0.8	1.0	
ATi1.5	1.9	1.5	1.9	7.2±1.5
BTi1.0	1.8	1.0	1.4	
ATi3.9	1.9	3.9	5.0	6.6±2.0
BTi3.9	1.8	3.9	4.3	6.9±1.5
ATi6.5	1.4	6.5	11.1	
Au/SiO$_2$	2^a			6.4±3.8
Au/TiO$_2$	1.8			11±6.8

a: nominal Au wt%; b: determined by TEM after calcination at 450°C followed by catalytic run

From comparison of the intended and the real Au and Ti loading it was clearly seen that in the preparation method A both the Au and the Ti components were successfully attached to the SiO$_2$. In the preparation method B, when first the Au/SiO$_2$ reference catalyst was prepared, the success of Ti introduction is obviously successful, since after the evaporation of water from the TALH solution, the Ti species should remain on the catalyst.

When gold sols are prepared from HAuCl$_4$ by citrate/tannic acid reduction, the gold nanoparticles are negatively charged as our Zeta potential measurements proved[21], therefore, the adsorption of the metal particles does not occur on SiO$_2$ due to charge repulsion between the stabilized metal particles and the silica surface charged negatively above pH=2-3. In our case the problem of the absence of attraction could be overcome with the aid of PDDA which provided positive surface charge by its preadsorption on silica. Since PDDA is a polycation, a monolayer coverage is expected to form spontaneously on negatively charged substrates such as silica, causing charge neutralization followed by charge reversal (positive surface charge) upon increasing the polymer bulk concentration[22,23,24]. The idea of using PDDA as a "binding agent" for our gold sols is originated from our earlier studies, when PDDA was used as stabilizer for Pd colloids[25]. It is worth mentioning that there was an optimum amount of PDDA, depending on the sol composition that facilitated the adsorption of Au particles. At high concentration of the polycation there may be free positively charged PDDA chains not only on the silica but in the liquid phase and around the Au particles as well, causing the adsorption step to fail.

The adsorption step is further complicated by the presence of the water-soluble titanium precursor, TALH that is partially dissociated into an anion and a NH$_4^+$ cation[26]. The advantage of TALH over the usual titania precursors such as alkoxides is its relative high resistance towards hydrolysis in aqueous media. In our case a relatively mild hydrolysis condition was set (at 60°C) for TALH in the presence of gold sol (preparation method A) or in the suspension of Au/SiO$_2$ (preparation method B) and there was no sign of color change or aggregation even after overnight stirring. When higher temperature (80-90°C) was applied, opacity and/or destabilization of gold sol occurred.

Concerning the components present in our system and the information listed in ref. [14], the scenario shown in Scheme 1 can be suggested for the formation of Au-TiO$_2$ nanostructures on Aerosil silica support by method A.
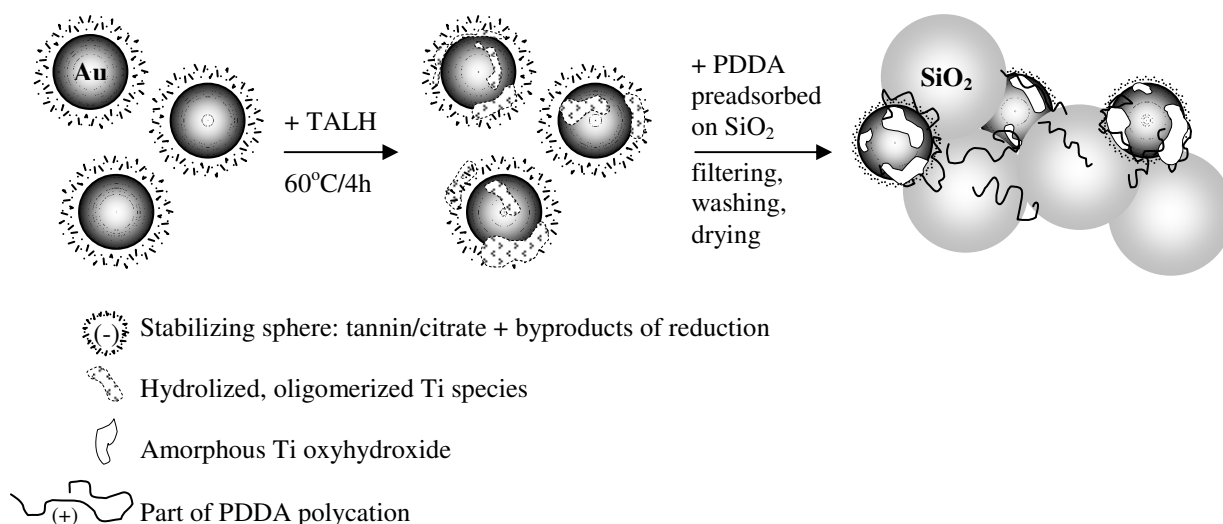
Scheme 1 The main steps of preparation method A with the suggested structures and interactions

We were not able to declare, in what form TALH was present before adsorption step, but we supposed the formation of Ti-oxy-hydroxyde oligomer species by the partial hydrolysis of TALH. We assume that hydrolyzed Ti species likely having positive surface charge[27] are mainly located

4

around the gold cores and Au particles must serve as nucleation sites for the condensation of Ti species. Furthermore, it is known that Ti(IV) ions in aqueous solution are able to coordinate to the phenolic oxygen groups of tannin[28] and to citrate ions[29]. Thus, in the sol adsorption step PDDA binds the gold particles covered by partially hydrolyzed tannic acid and Ti species to the silica surface, since association of both with positively charged polyelectrolytes such as PDDA can be expected[30, 31, 32, 33].

In the case of the preparation method B the gold nanoparticles are located already on silica when the partial hydrolysis of TALH takes place. Thus, TALH and other titania species may be deposited not only on Au but on silica as well. Drying and the subsequent calcination in air remove the carbonaceous deposits from the catalysts and transform all Ti species into TiO_2 (or TiO_x).

3.2. Structure of the catalysts: particle size and distribution of Ti species

TEM image of Au/SiO_2 reference is shown in Figure 1. Gold particles are nicely distributed on the surface of SiO_2. From the particle size data presented in Table 1 it is clearly seen that Ti deposition does not cause any obvious increase in Au diameter.
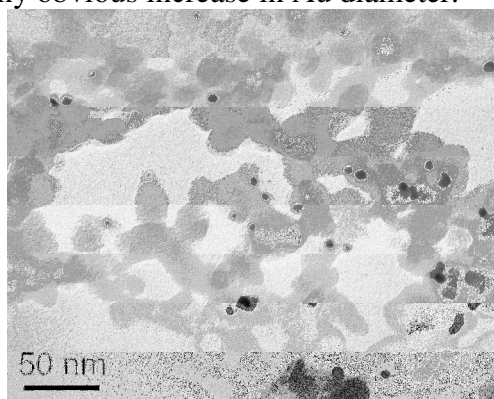

Figure 1 TEM image of Au/SiO_2 after calcination at 450^oC

In any of our TEM pictures taken of the Ti containing samples there was no sign of titania particles, only EDS proved the presence of Ti in the catalysts. Using EDX spectra collected from 20-50 nm diameter spots we detected some differences between the two preparation methods, especially at lower Ti contents concerning the location of Ti. In the case of method A at low TiO_2 content (ATi1.5) the analysis did not reveal the presence of Ti on bare SiO_2 without gold, however, at higher TiO_2 content Ti signal could be observed at certain spots of the sample without detecting Au. It means that a specific attraction, ensured by the stabilizing sphere of tannic acid and citrate, dictates the bonding of TALH and/or the hydrolyzed and polymerized titanium species to Au particles already in liquid phase and so Ti is enriched on/around gold nanoparticles. When TALH is added to the preformed Au/SiO_2 sample (method B) Ti could be detected both on silica and gold.

To further clarify the question of titania location HRTEM investigations were carried out. The HRTEM images of ATi1.5 sample in Figure 2 a) and b) evidence a TiO_2 decoration on Au that is a few layer thick (but according to EDS measurements may not homogeneously cover all Au particles) and comprises partially ordered anatase (JCPDS 21-1272, [101] interplanar spacing is 0.35 nm) and β-TiO_2 phases phase (JCPDS 35-0088, [200] spacing is 0.579 nm). In the case of ATi3.9 (~4 wt% TiO_2 content) very thin crystalline titania overlayer/sheets or islands of titania (both anatase and β-TiO_2) appeared on the Au particles and also on silica after calcination at 450^oC as it can be seen in Figure 2 c). Thus, we can accept the existence of surface TiO_2 that decorates and surrounds the Au particles providing an increased Au-TiO_2 interfacial area.

Looking at the Au size and its distribution (shown in ref. [14]), which is reflected in the standard deviations of average size, we can declare that TiO_2 decoration stabilizes gold particles on SiO_2 against sintering compared to Au/TiO_2 and Au/SiO_2 references. Tsubota et al.[34] also observed

that the size of Au particles after 400°C calcination increased on a pure titania support, however, it did not change in the case of a titania-coated silica aerogel.
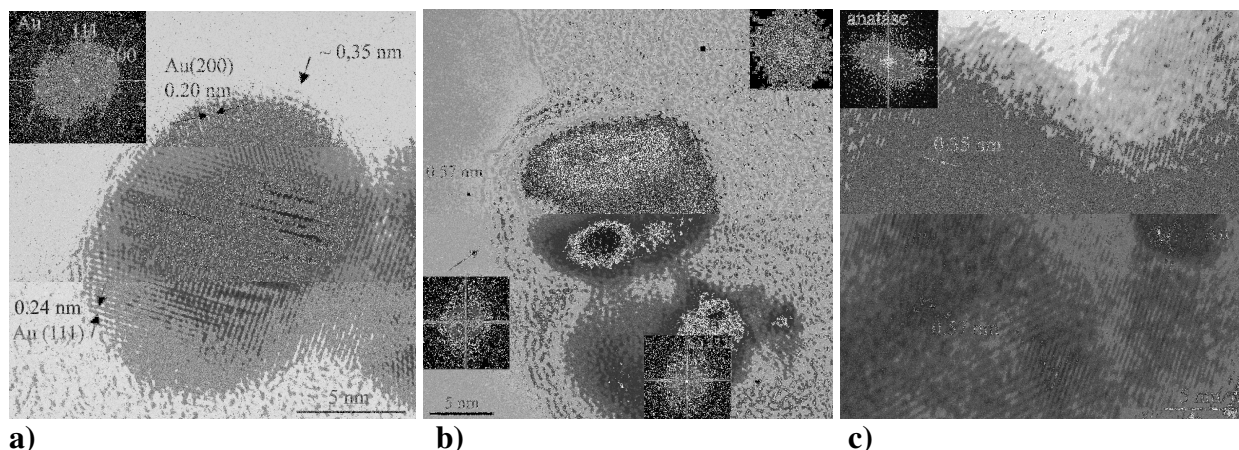

a)   b)   c)

Figure 2 HRTEM picture of a) Au particle in ATi1.5 covered by titania patches of anatase structure; b) Au particles in ATi1.5 covered by β-TiO$_2$ phase and c) HRTEM picture of ATi3.9 with both titania structures present

3.3. Catalytic properties

Blank TiO$_2$/SiO$_2$ sample was prepared to check the activity of dispersed TiO$_2$ phase without Au but the sample exhibited very low oxidation activity: CO oxidation started at 300°C and up to 450°C only 17 % conversion was achieved. The catalytic reaction was proved to be the most sensitive test to show the intimate contact of nanosized TiO$_2$ and Au. The activity of the sample with TiO$_2$ content as low as 0.2wt% was already higher than that of Au/SiO$_2$.
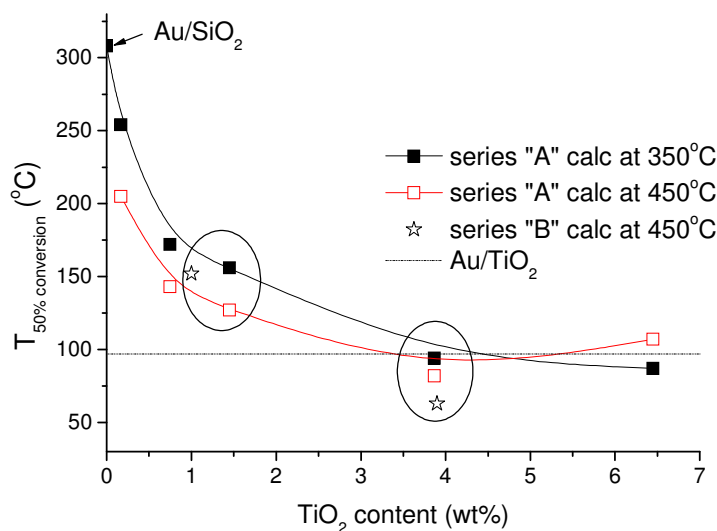

Figure 3 The temperature of 50% CO conversion versus TiO$_2$ content. Dotted line represents T$_{50\%}$ of Au/TiO$_2$

Figure 3 shows that as the Ti content increased, the activity greatly increased, viz. the temperature of 50% CO conversion was strongly lowered until it reached a broad minimum. The samples containing ~4 wt% TiO$_2$ have higher activity than Au/TiO$_2$ which proves the formation of large and active Au-TiO$_2$ interface and suggests that the decorating patches of nanosize TiO$_2$ in contact with gold must have different oxidizing properties than bulk TiO$_2$[35,36]. We observed very similar phenomena when Au sol was deposited on SiO$_2$ containing 5 wt% highly dispersed TiO$_2$

(Au/5%TiO$_2$-SiO$_2$). Structural and catalytic studies revealed that the superior intrinsic activity of Au sites over Ti-O-Si units must be responsible for the high activity compared to the case when Au is over Ti-O-Ti units[13].

At the first glance the similar activity of BTi3.9 compared to ATi3.9 is somewhat surprising, although, the calcination pretreatment at 450°C may diminish the structural differences between the samples prepared by method A and B. If all the Ti evenly covered the catalyst surface in the case of method B, there would be a very low coverage of TiO$_x$ on gold parts, consequently, lower activity should be observed. The fact that method B results in catalyst with similar activity as method A suggests that the deposition of Ti species during method B might also be governed by the interactions between the partially hydrolyzed TALH, tannic acid and PDDA and results in similar morphology as method A.

These results inspired us to conduct further research using ATi3.9, Au/5%TiO$_2$-SiO$_2$ and mechanical mixtures of Au/SiO$_2$ + Au/TiO$_2$ reference samples in 95/5 ratio[37]. In fabrication of Au/5%TiO$_2$-SiO$_2$ Au introduction was done by sol deposition onto 5%TiO$_2$-SiO$_2$ support prepared by surface OH induced hydrolysis of Ti-isopropoxide[13]. A portion of the mechanical mixture was suspended in water, another portion was calcined in air separately and then mixed and suspended in water. Final samples were compared by Au particle size and CO oxidation. The results revealed that in the suspension of TiO$_2$ and SiO$_2$ the intimate contact of the two types hydrated oxide particles enhances the possibility of Si-O-Ti formation during calcination and the Au particles may be locally redistributed and segregated towards TiO$_2$ surface. The preferential migration of Au towards TiO$_2$ or SiO$_2$/TiO$_2$ perimeter seems to be controlled by the PDDA and tannic acid/citrate present in the system, because when all organic stabilizers and the PDDA were removed by calcination before mechanical mixing, in the subsequently prepared aqueous suspension the Au particles aggregated causing low activity.

The most active TiO$_2$ promoted catalysts (ATi3.9 and BTi3.9) were tested in PROX reaction (1%CO+1%O$_2$+62%H$_2$ in He gas mixture) after calcination and compared to the analogoues Au/TiO$_2$ [21]. On all these samples relatively low selectivity of CO (below 50%) is characteristic, especially above 20-25% O$_2$ conversion, which means that the maximum CO conversion reached was below 40%. The promoted samples were more active both under PROX conditions and CO oxidation (ATi3.9>BTi3.9), but because of the accelerating H$_2$ oxidation above 80-100°C, when O$_2$ conversion was approaching 100%, CO conversion decreased. Au/TiO$_2$ behaved similarly at higher temperature (at 120-130°C). The maximum CO conversion could not be increased significantly in the promoted samples but it was reached at lower temperature.

3.4. Application of SBA-15 support in the case of Au-TiO$_2$/SiO$_2$ systems[38]

Mesoporous silica host is a promising support able to hinder metal particle aggregation when they are located inside the pores. SBA-15 was applied as support for Au instead of non porous Aerosil silica in our investigations and preparation method B was applied to introduce TiO$_2$ modifier from TALH solution. This sample can be considered as TiO$_2$/Au/SBA prepared by method B. The differences compared to the Au-TiO$_2$/Aerosil samples discussed above are that i) the parent Au sol with d$_{Au}$=2.7 nm was prepared in a different way, by NaBH$_4$ reduction in the presence of PVA, ii) the support is mesoporous thus particle size increase and diffusion of materials can be limited to some extent and iii) the adsorption of Au sol was done at low pH without the application of PDDA. The calcined TiO$_2$/Au/SBA sample had similar activity in CO oxidation as the reference Au/SBA thus the introduction of Ti component did not produce sufficient and active Au-TiO$_2$ interface (pore blocking could happen, however the crystallite size of TiO2 was much smaller than the pore size according to XRD results). Zeta potential measurements proved that the surface charge of Au/SBA in aqueous suspension is more negative than that of SBA-15 itself, this means that the surface of Au particles is more negative than the surrounding support surface. During the impregnation of Au/SBA with TALH, the deposition of negatively charged Ti precursor was likely

favoured on the less negative pure SBA-15 surface instead of Au particles, thus Au-TiO$_2$ interface was hardly produced[38].

4. Investigation of the Au-CeO$_2$/SiO$_2$ systems

Ceria is one of the most promising supports for gold since it can provide reactive oxygen via forming surface and bulk vacancies through redox processes involving the Ce^{4+}/Ce^{3+} couple. Depending on the morphology (preparation method) of ceria, different catalytic activities can be obtained, which can be related for example even to the exposed crystal planes of ceria nanocrystals[39].

The synergetic effect of the Au-CeO$_2$ interface was mostly investigated in the "usual" way, when small amount of CeO$_2$ is used to modify the otherwise inactive support such as silica, and finally Au is deposited onto this CeO$_2$/SiO$_2$ support. However, we must be careful when assigning any catalytic behavior solely to the effect of oxide loading and structure, if the Au particle size or oxidation state differs significantly in the catalyst samples investigated[40]. Qian and co-workers[41] studied the effect of CeO$_2$ microstructures present in Au/CeO$_2$/SiO$_2$. They experienced that Au supported on CeO$_2$/SiO$_2$ prepared by wet impregnation and calcined at only 200°C was the most active sample, where Au nanoparticles were dispersed on the CeO$_2$ aggregates on SiO$_2$ and the pure SiO$_2$ surface, as well. The inhomogeneous distribution of Au on CeO$_2$-containing hexagonal mesoporous silica (HMS) support was seen by Castano and co-workers, as well[42]. When Ce-modification of the mesoporous silica was done by direct synthesis or impregnation, the impregnated catalyst was better regarding the activity. Higher Au dispersion, highest content of Au^o and larger degree of CeO$_2$ coverage on HMS (more effective oxygen mobility, higher redox ability) were suggested as reasons[43].

Thus, we can conclude that the preparation method and the pre-treatment conditions are of vital importance, when the effect of CeO$_2$ loading on the properties of Au-CeO$_2$ interface is to be studied using inactive SiO$_2$ oxide support to provide high surface area against sintering. If there are Au particles not in contact with CeO$_2$ but with SiO$_2$, the overall activity measured will be the sum of activities originating from Au/SiO$_2$ and Au/CeO$_2$-SiO$_2$ areas present in the sample.

According to the "inverse catalyst strategy" we continued our research with the intention to selectively produce CeO$_2$ decoration on Au nanoparticles. The idea of post-addition of CeO$_x$ modifier to Au catalyst was realized by Senanayake and co-workers[44] as well, however, they investigated Au(111) model surfaces in water-gas shift reaction (WGS). The total encapsulation of Au by ceria was accomplished by using microemulsion method, but no activity was observed in water-gas shift reaction. The authors suggested that the activity depends rather on electronic aspects of metal-ceria interface instead of oxygen mobility of the ceria oxide shell[45].

4.1. Formation of Au-CeO$_2$ nanostructures on silica support

Au and Ce containing samples were prepared by both method A and B with different Ce-loadings. We should mention that, when the largest amount of Ce(III) nitrate was added to the Au sol during method A, destabilization of the colloidal system happened and red precipitate with hardly observable tiny particles formed. Additional citrate seemed to dissolve this precipitate. The next sample with less Ce-content was prepared with more care, thus, the addition of Ce(III) nitrate solution to the Au sol was done drop by drop and finally some additional citrate was added and no change of colour was observed this time and the sol was stable on the following days as well.

Table 2 contains data of metal loading of the samples together with the particle size determined by TEM and catalytic data which will be discussed later on. It is certainly eye-catching that the final CeO$_2$ content of samples prepared by method A is very low and more than 10 times less than the intended values (0.5wt%, 2.5wt%, 7.5wt%). Thus, we prepared low loaded samples by method B as well to be able to compare catalysts synthesized by the two methods at similar Ce loadings.

Table 2 Metal loading, temperature of 50% CO conversion (CO/O$_2$=1/18) and Au particle size of the samples

Sample	Au content (wt%)	CeO$_2$ content (wt%)	T$_{50\%}$ (°C)		Au particle size[b] (nm)
			after calc. at 300°C	after calc. at 450°C	
ACe0.04	2.00[a]	0.04		121	6.30±1.45
ACe0.08	1.79	0.08	138	85	-
ACe0.16	1.83	0.16	76	83	8.07±3.44
BCe0.06	2.00[a]	0.06	-	140	-
BCe0.11	2.00[a]	0.11	-	70	-
BCe0.60	1.96	0.60	50	48	5.73±1.92
BCe1.14	1.84	1.14	49	47	-
BCe2.64	1.88	2.64	44	44	6.57±1.65
BCe7.40	1.68	7.40	51	40	7.15±1.75
Au/SiO$_2$	2.00[a]	0	-	401	6.37±3.78
Au/CeO$_2$	2.00[a]	98	74	-	8.00±3.81

a: nominal value

b: determined by TEM after calcination at 450°C and catalytic run

Let us consider what happens at the addition of cerium nitrate to the parent Au sol which has a pH=6.5 containing hydrolyzed tannin and citrate and all the byproducts of reduction. For the preparation of crystalline CeO$_2$ nanoparticles the main synthesis method is the hydrothermal route and if the starting precursor is Ce(III), it is usually oxidized to Ce(IV) by the presence of air. Due to the addition of base Ce(OH)$_4$ forms, then Ce(OH)$_4$ nucleation and growth takes place, and finally the Ce(OH)$_4$ particles formed dehydrate into CeO$_2$ during heat treatment[46,47,48]. In our case it was not ascertained whether or not Ce-nitrate hydrolyzed in our reaction conditions. Macroscopic particle aggregation which was observed at the highest cerium concentration does not necessarily mean the formation of hydroxide precipitate but it may reflect only charge neutralization and flocculation of Ce(III)-tannin-citrate complexes since both reducing/stabilizing agents present in the Au sol are able to complex metal ions[49] such as Ce(III),[50] or stabilize CeO$_2$ or Ce-hydroxide particles, as well[51,52]. The pH of the Au sol was 6.5 which is still acidic so we rather suggest that no or only partial hydrolysis happened to Ce-nitrate in our experiments and most of Ce(III) was bound in a chelate complex with tannin (gallic acid) and citrate. At lower Ce-nitrate concentration complete charge neutralization and so macroscopic precipitation did not happen between the anionic organic molecules and cerium ions.

In the subsequent adsorption step, PDDA was used again to recharge the SiO$_2$ surface to be able to bind Au particles covered by negative stabilizing sphere. The final low Ce content of samples prepared by method A reflects that Ce species (any kind of them) do not favour the positively charged polyelectrolyte covered solid and they rather remain in liquid phase in the filtrate associated with hydrolyzed tannin and citrate ions. The highest negative charge and the highest concentration of complexing agents for Ce(III) is located around the Au particles, that is why the relatively low Ce concentration is expected to be concentrated around Au.

In the case of method B the gold nanoparticles were located already on silica when Ce(III) nitrate was added. The samples were washed to remove the majority of organic and inorganic residues and dried at 60°C before Ce addition, however, negatively charged residual-shell around the gold can be expected which may localize a part of added Ce-nitrate.

In both methods the final evolution of Au-CeO$_2$ nanostructures takes place during calcination in air when all Ce species transform into CeO$_x$/CeO$_2$.

4.2. Structure of the catalysts: particle size and distribution of Ce species

In whatever form Ce species are present after drying, calcination pretreatment to remove organic moieties transforms them into Ce-oxide. X-ray diffraction pattern of BCe7.40 and BCe2.64 detected crystalline CeO_2 phases with 5-6 nm. Table 2 presents Au particle sizes determined by TEM and the standard deviations which are characteristic of the particle size distribution. The particle sizes of all the samples do not differ significantly, they range between 5.7 nm and 8.1 nm which is not the interval of the usual sudden change in activity with Au dispersion ($d_{Au} \sim$ 0-5 nm). It is clearly seen that ceria modification induces a kind of stabilization effect since the $Au-CeO_2-SiO_2$ systems are more monodisperse, except, no wonder, for ACe0.16 which was the sample obtained by the adsorption of previously destabilized Au-Ce composite sol.

HRTEM provided further information on the location, size, and structure of the promoting oxide. The HRTEM micrographs of sample BCe7.40 are shown in Figure 4(a) and (b). Figure 4(a) reveals the presence of nanosize CeO_2 particles, in contact with the Au nanocrystals surfaces. Two thin slabs with fringes can be observed partly covering the Au particles in the inset of the figure. The fringe period (0.32 nm) corresponds to the (111) lattice spacing of cubic CeO_2. Far from the Au particles, the pure SiO_2 surface is also covered by thin CeO_2 particles of 5-15 nm size as shown in Figure 4 (b).
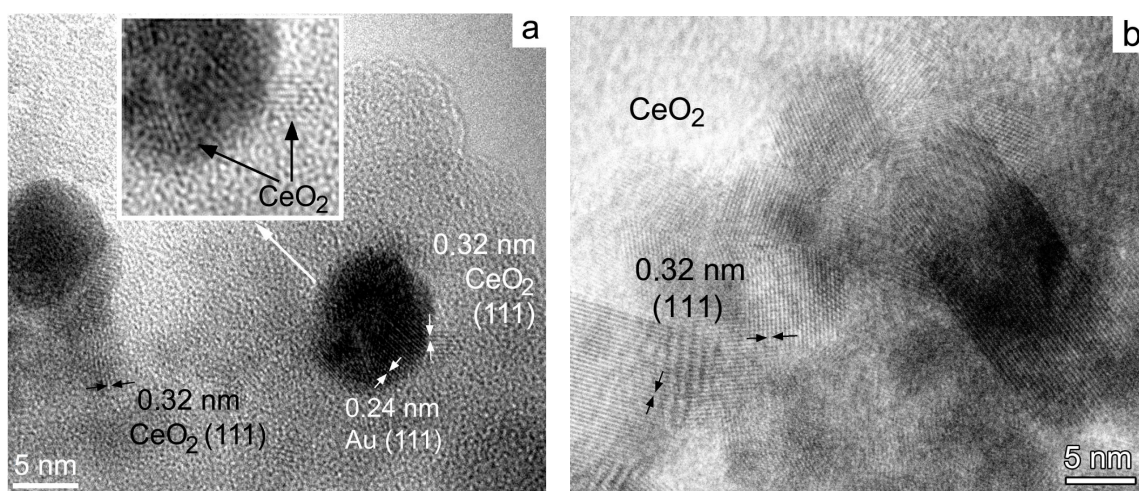

Figure 4 HRTEM of BCe7.40 with 7.4 wt% CeO_2. The 0.32nm period lattice fringes represent CeO_2 crystals both attached to the Au particles (a), and located, in large patches, on the SiO_2 (b).

The sample BCe2.64 also contained CeO_2 particles both in contact with and separated from the Au, but the amount of separate CeO_2 was less due to the lower Ce-content (images are in the attached manuscript[53]). As we go further to less Ce-content (BCe0.60), HRTEM measurements show that the CeO_2 appears mostly on or nearby the Au surface, while the silica is depleted in CeO_2 (the images are also seen in manuscript ref. [53]).

To reveal the distribution of CeO_2 at extreme low cerium contents is of crucial importance, because theoretically it is very easy to locate this amount of Ce-oxide on the high surface area Aerosil SiO_2 without even any contact with Au particles. With this aim, a sample prepared by method A (0.04wt% Ce) was also investigated. HRTEM and EELS found no trace of Ce-oxide on silica, however, it gave definite proof of CeO_2 associated to Au (the existence of $Au-CeO_2$ interface) as it is presented in Figure 5. Fig. 5 (a), (b) and (c) show the unfiltered HRTEM image, the EELS Ce-map and the enlarged frame "c" from (a), respectively. The bright contrast in the Ce map (b) indicates a distribution of Ce exclusively around/on the Au particles (see also the arrows). No remarkable signal of Ce was detected apart from the Au crystals. Furthermore, in Figure 5 (c) a single Au particle is seen (enlarged frame from (a)) with the lattice fringes of CeO_2 nanoparticles on its surface.

We calculated the possible maximum coverage of CeO_2 exclusively on Au surface assuming 2 wt% Au and 0.04 wt% CeO_2 content and d_{Au}=6 nm size particles. We obtained that at such a low Ce-content only 17% of the Au surface can be covered by CeO_2. If ceria is present in multiple layers, this number is even smaller.
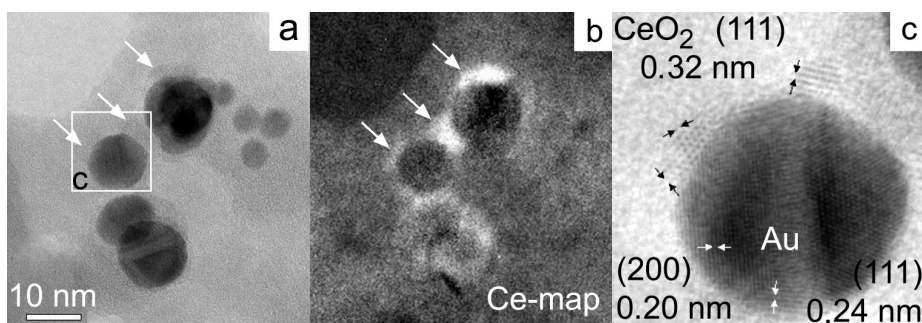

Figure 5 Unfiltered micrograph (a) and EELS Ce map (b) of sample ACe0.04 with 0.04 wt% CeO_2. The bright contrast in the Ce map (b) marks regions that contain Ce. The enlarged image (c) shows CeO_2 particles (0.32nm lattice spacing) on the Au crystal (from the center of (a)). Practically no CeO_2 was found apart from Au.

Considering all experimental results, XRD and HRTEM measurements proved the presence of crystalline ~ 5 nm size CeO_2 particles/domains in our samples. Depending on the Ce-loading and preparation method, ceria can be found on the bare silica surface and on the Au nanoparticles as well. The localized oxide promotion of gold is greatly accomplished, since it seems that independent of the preparation method, gold surface is somehow saturated by ceria first, then the increase of Ce-loading causes Ce species spread over the support surface, as well, just like in the case of Ti-modification. Full coverage of a single Au particle by ceria, viz. core-shell structures were not detected.

4.3. Catalytic properties
CO oxidation with CO/O_2=1/18 ratio was used as a highly sensitive tool to test the presence of Au-CeO_2 active interface. The catalytic measurements were conducted after calcination treatments at 300°C or 450°C.

Figure 6 summarizes the CO oxidation activity of the samples, viz., the temperatures where 50% CO conversion was achieved ($T_{50\%}$) as a function of ceria content. Data obtained after different calcination temperatures and different preparation methods are distinguished, but surprisingly lay on the same line, which sharply increases at CeO_2<0.5 wt% meaning the decline of activity. The dotted line at 74 °C in Figure 6 indicates the activity of the reference Au/CeO_2 sample. We can state that enhanced catalytic activity of CeO_2-modified samples was found compared to Au/CeO_2 reference sample at as low as 0.6wt% of CeO_2 loading already. The very little 0.04 wt% CeO_2-content on the other side makes ACe0.04 sample already a more efficient catalyst than the reference Au/SiO_2.

The difference between the activities of the samples is much better discernable looking at Figure 7 where a few representative conversion curves obtained after calcination pretreatment at 450°C are plotted against temperature. The main issue is that at larger than 0.6wt% CeO_2-content (by method B) there is practically no difference between the catalysts. Furthermore, there is a slight difference in favor of method A, because ACe0.04 sample exhibits better activity than BCe0.06 in spite of the higher Ce-content of the latter. We tentatively suggest that, when Ce precursor is added to the sol, the stabilizing sphere around Au is full and attracts more Ce species to be attached and complexed there than the one after washing off most of organic materials and drying (what applies for method B). Still it is surprising that washing leaves a sufficient part of negatively charged stabilizing sphere on the surface of Au and so when Ce-nitrate added during preparation method B

to the suspension, it is bound first to the Au particles as HRTEM and catalytic studies proved. Otherwise, if 0.06 wt% CeO_2 were homogeneously dispersed on silica surface it would not provide a catalyst with $T_{50\%}=140^{o}C$ (note that $T_{50\%}=401^{o}C$ for Au/SiO_2).
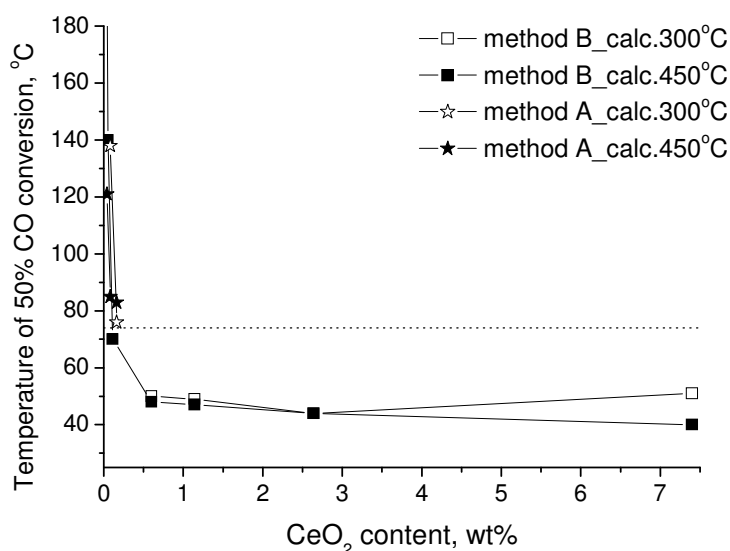

Figure 6 CO oxidation activity of the samples prepared by method A and B: the temperatures where 50% CO conversion was achieved ($T_{50\%}$) as a function of ceria content. $350^{o}C$ calcination / temperature is signed with empty, $450^{o}C$ pretreatment temperature is signed with full symbols)
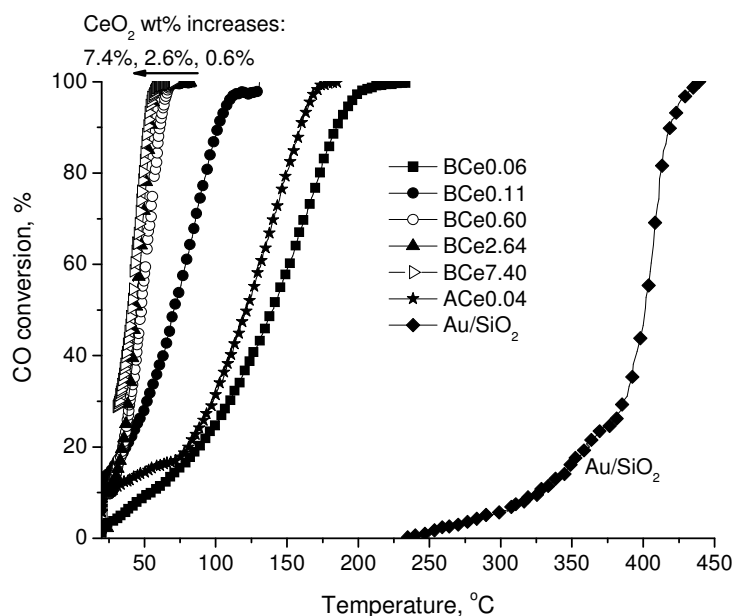

Figure 7 Representative conversion curves of samples prepared by method A and B versus reaction temperature. The data were obtained after calcination pretreatment at $450^{o}C$. Note the extremely similar curves at CeO_2 content >0.6wt% for samples prepared by method B.

Considering the results of XRD, TEM and catalytic tests we are definite to say that nanosize, thin CeO_2 domains that are localized around Au particles play the crucial role in the reaction, and CeO_2 islands far from Au particles are not able to influence or enhance catalytic activity through the well-known oxygen storage and release capacity to a significant extent. The CeO_2 coverage on Au is somewhat limited due to the complexing capacity of stabilizing sphere, this is why at higher Ce-

12

loading even more and more ceria is deposited on the bare silica, additional activity increase cannot be observed or it is only negligible.

According to the literature references cited in ref. [53] in Catalytic Properties section, we tentatively suggest that our thin CeO_2 patches in close contact with Au nanoparticles may contain large amount of Ce(III) ions and so many oxygen defect sites, which in turn enhance oxidation ability compared to the bulk, commercial CeO_2 particles. Special electronic interaction may exist between the contacting few layer thick CeO_2 patches and the Au particle. Furthermore, the contact area between Au and nanosize CeO_2 islands must be larger than the interface between the same Au particles and the bulky ceria particles of ceria nanopowder.

We can conclude that compared to TiO_2-Au/SiO_2 system, where the activity reached the activity of the reference Au/TiO_2 sample only at 4wt% TiO_2-loading, here, in the case of CeO_2-Au/SiO_2 systems a small amount of Ce (0.16wt% CeO_2) was enough to reach the activity of the Au/CeO_2 reference sample, which was highly exceeded by the samples with CeO_2 content above 0.6 wt%.

Calcined BCe0.6, BCe7.4 and ACe0.08 were tested also in PROX reaction in comparison with the analogous Au/CeO_2. The promoted samples were significantly more active in the simple CO oxidation and were less efficient in PROX than Au/CeO_2. The latter one could convert more than 90% of CO at about 110°C, while BCe0.6 and BCe7.4 presented lower maximum CO conversion (54% and 67%, respectively) at somewhat higher temperature (137°C and 138°C, respectively). Even ACe0.08, the least active in CO oxidation produced higher maximum CO conversion (71% at 160°C) than the catalyst prepared by method B. The hydrogen oxidation is more favoured on the promoted samples than on Au/CeO_2. The effect of reductive pretretament (350°C in H_2) on PROX performance was investigated on BCe0.6, and much lower CO oxidation selectivity was achieved. In a repeated calcination treatment the original PROX performance could almost be regained.

4.4. Application of SBA-15 support in the case of Au-CeO$_2$/SiO$_2$ systems[38]

Post-modification of Au/SBA-15 with 10% CeO_2 was carried out in our laboratory as well by impregnation of Au/SBA with Ce(III) nitrate solution (resulting CeO_2/Au/SBA prepared by method B). The sample had outstanding activity in CO oxidation compared to the reference Au/CeO_2 with basically the same Au particles of 5-5.6 nm. Beside the differences compared to the Au-CeO_2/Aerosil samples (that parent Au sol was stabilized by polyvinylalcohol, mesoporous support was used, no PDDA was applied at the adsorption step), we can draw similar conclusion on the effect of nanosize CeO_2 decoration on gold. Zeta potencial measurements proved that the surface charge of Au/SBA in aqueous suspension was more negative than that of SBA-15 itself, this means that the surface of Au particles was more negative than the surrounding support surface. Thus, during the impregnation of Au/SBA with Ce nitrate, the positive Ce(III) ions are rather attracted by the Au surface. The nanostructured Au-CeO_2 interface formed is more active than the interface between Au and the support CeO_2 of about 23 nm crystallite size.

5. Investigation of the Au-CuO/SiO$_2$ systems

5.1. Introduction, background

When the research proposal was written in 2005, there were only a few literature references, to the best of my knowledge, about the simultaneous application of supported CuO (Cu) and gold nanoparticles for CO oxidation purposes. Since then several publications have been written about similar systems due to the scientific interest emerged, but still the area of combination of Cu and Au for oxidation reactions deserves deeper investigations. The results shown here are not complete, further work is needed to explain all the interesting effects observed.

CuO-CeO_2 mixed oxides were already tested and proved to be very good and selective candidates at certain conditions for the CO oxidation and the preferential CO oxidation[54]. Well dispersed CuO phase[55,56] and stable solid solutions of CeO_2-CuO or CeO_2-CuO comprising copper

oxide clusters strongly associated with ceria were proposed as active sites for the reaction[57,58]. Bulk CuO was supposed not to contribute to the activity.

Combination of gold and copper oxide supported on Al_2O_3 surface was studied by Nieuwenhuys and co-workers in CO oxidation[59] and in total oxidation of propene[60]. The catalysts were prepared by deposition precipitation (DP) of Au and Cu precursors or by impregnation of the alumina with Cu nitrate followed by DP of gold. Calcination was applied to render copper species into oxide form. CO oxidation was suggested to take place between the adsorbed CO species bound to Au and O species activated on copper oxide at the Au-oxide perimeter. Oxygen vacancies and at higher temperature also the lattice oxygen were suggested to play important role in supplying oxygen for the reaction. Total oxidation of propene, however, was found more efficiently catalyzed by the $Au/12wt\%CuO/Al_2O_3$ sample which contained more crystalline CuO than $Au/6wt\%CuO/Al_2O_3$ with the same total gold surface (but not Au particle size). This finding is in contradiction with the above mentioned role of highly dispersed CuO phase in CeO_2-CuO oxides.

Copper in metallic form or rather in bimetallic AuCu particles was also found to be active in CO oxidation or PROX. AuCu alloy nanoparticles with Au core and Cu shell were produced by a two step preparation method using silica support. First, reduction of $HAuCl_4$ with $NaBH_4$ was done in the suspension of surface-modified SiO_2, then the same reduction step was repeated with different amounts of Cu-nitrate, finally the sample was calcined and reduced. At low Cu loading (Au:Cu=20:1), there was not enough Cu to form a monolayer coverage, so Cu oxide may have just formed some patches on the gold core during calcination and upon reduction the metallic Cu diffused into the crystalline structure of gold to form AuCu. The composition of alloy nanoparticles was fluctuating (d spacings were different for the particles investigated by HRTEM). These AuCu bimetallic particles were found to be more active and selective than Au or Cu in the temperature range investigated (30-80°C), which means the Cu component in the AuCu catalysts facilitated the activation of oxygen at low temperature in a different way than Cu/SiO_2 did[61]. The above preparation method was applied to produce SBA supported AuCu catalysts, as well. In this case the discrepancy between XRD results and ICP data suggested that not all the Cu in the catalyst was alloyed with gold. If the temperature is higher one has to think of the influence of a possibly oxidizing atmosphere during CO oxidation (which of course depends on the O_2 concentration). Indeed, in CO oxidation above 300°C phase separation, CuO_x segregation happened. In situ EPR measurements proved that majority of Cu^o in the AuCu alloy was oxidized to Cu^+, but only a small part of Cu^o was further oxidised to Cu^{2+} during CO oxidation. Furthermore, in situ XANES measurements revealed that a part of copper oxide that strongly interacted with the support was difficult to reduce and it remained Cu^+ (Cu_2O) even after reduction (and limited the aggregation of bimetallic particles)[62]. Thus, we can see that the original metallic state of Cu can be modified during catalytic reaction, and so the active sites can vary depending on the actual reaction conditions.

The effect of metallic Cu on Au/Al_2O_3 prepared by DP method followed by only reduction treatment was investigated by Mozer and co-workers[63]. Addition of only 0.5wt% Cu was beneficial in catalytic activity (PROX), but more Cu seemed to block Au sites. Beside geometric effect, electron transfer from Cu to Au were suggested to govern the adsorption of reactants and so the catalytic behaviour[63,64].

A surprising stable metallic alloy was reported to form during reduction of Au salt and Cu nitrate with $NaBH_4$ in the presence of dodecanethiol (stabilizer) in toluene. $AuCu/TiO_2$ was the final supported sample which was calcined at different temperatures. After calcination at 400°C AuCu remained metallic (XPS) with fcc lattice constant values. Part of the copper atoms did not alloy, but remained as small clusters or were segregated on the surface of alloy particles. At higher calcination temperature phase segregation started; surface enrichment in Cu was seen for the bimetallic samples calcined at 600°C[65].

We can conclude based on the above literature references that depending on the preparation method, particle size, support nature, metal loading, reaction condition, etc., the state of copper species can be greatly varied. Since our aim was to form small CuO patches on the surface of gold

nanoparticles and investigate the inverse system formed, we applied only calcination treatment at 450°C before the first catalytic measurements for the removal of organic residues and for the production of copper oxide modifier.

5.2. Formation of Au-CuO$_x$ nanostructures on silica support

Preparation of the samples was done according to the method A and B previously described in details. The Cu precursor was Cu(II) nitrate solution. One sample was produced with method A with a nominal CuO content of 0.12 wt% (Au/Cu=10) and 3 samples were prepared by method B with 1 wt% CuO, 1 wt% CuO + 1 wt% CeO$_2$ and 4 wt% CuO content (nominal values). During method A additional Na citrate was introduced together with Cu nitrate to prevent hydroxide formation via complex formation with citrate. Reference Cu/SiO$_2$ prepared by impregnation of SiO$_2$ with Cu(II)-nitrate with the addition of citrate and PDDA and Au/SiO$_2$ produced by Au sol adsorption on Aerosil 200 with the aid of PDDA were used as comparison. Table 3 summarizes the size of particles measured by TEM and the Cu content of the samples determined by XRF and expressed in CuO wt% (the numbers in the sample names refer to the actual CuO loading). Au content was the nominal 2 wt% in all cases.

Table 3 Au particle size determined by TEM and copper content of the samples

Sample	d$_{TEM}$ of Au (nm)[a]	CuO (CeO$_2$) content wt%
BCu0.88Ce1.06	5.9±1.6	0.88 (1.06)
BCu1.04	12.6±4.6	1.04
BCu3.72	6.2±3.4 (6.6±2.9)[b]	3.72
ACu0.08	5.1±1.5 (5.5±1.8)[b]	0.08
CuO/SiO$_2$	-	4.00
Au/SiO$_2$	6.4±3.8	0

a: after calcination/450°C and CO oxidation reaction (CO/O$_2$=18); b: at the end of PROX measurements which comprises calc/450°C, PROX reactions, CO oxidation reactions (CO/O$_2$=1/1), reduction treatment in H$_2$/450°C, PROX cycles and finally CO oxidation (CO/O$_2$=1/1) cycles

First we should discuss the success of introduction of the Cu modifier by method A, because according to previous experience it can be either very limited (in the case of Au-CeO$_2$ systems) or relatively easy (in the case of Au-TiO$_2$ systems). In the present case we can conclude that large portion, but not all the copper was supported on the silica surface together with Au particles or separately. Liu and co-workers[61], when preparing Cu nanoparticles with NaBH$_4$ on the surface of APTES-modified silica also experienced difficulty in loading of all Cu, but the reasons were not discussed. The distribution of this small amount of Cu species on the surface of the catalyst must be reflected in the catalytic behaviour, because it can cause difference compared to the reference Au/SiO$_2$ only if the Cu component (Cu oxide or metal?) is in contact with Au. The final lower CuO content of sample prepared by method A reflects that a small part of Cu species (complexes) must remain in liquid phase in the filtrate probably associated with hydrolyzed tannin and citrate ions and do not attach to the positively charged PDDA containing surface due to electronic repulsion effects.

In the case of method B the gold nanoparticles were located already on silica when Cu(II) nitrate and in one case Ce(III) nitrate was added. Copper complexes may be formed with the remaining stabilizing ligands still present around Au or copper hydroxide or oxyhydroxide can be produced during the evaporation of water. It is known that depending on the pH and the concentration of components, etc. Cu^{2+} forms negatively charged or uncharged monomer or dimer complexes with citrate ions[66], thus citrate is able to prevent formation of Cu(OH)$_2$ that otherwise

would form[67]. However, in this case additional citrate was not added concomitant with Cu(II) nitrate.

In the case of both methods the final evolution of Au-CuO nanostructures takes place during calcination in air, when all Cu species are expected to transform into CuO_x.

5.3. Structure of the catalysts: particle size, distribution and reducibility of Cu species

TPR measurements were carried out after calcination pretreatment at 450^oC with all calcined samples. Figure 8 shows the TPR curves of samples produced by method B and that of CuO/SiO_2 reference, on ACu0.08 sample measurable hydrogen consumption was not detected. A single unresolved peak can be seen for all the samples at around $260-270^oC$ which is assigned to the reduction of copper oxide species[56, 60]. The simultaneous presence of CeO_2 does not seem to promote or influence the reduction behaviour (see BCu0.88Ce1.06), nor does Au (compare CuO/SiO_2 and the others).
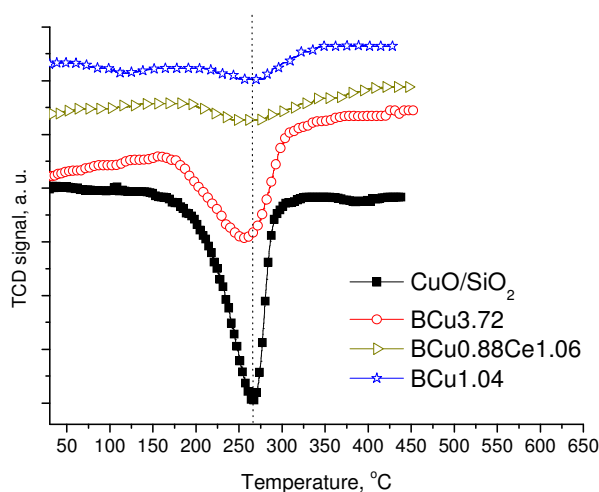

Figure 8 TPR curves obtained after calcination treatment at 450^oC in 5% O_2/He

Two samples were measured by XRD after calcination/450^oC and CO oxidation reaction ($CO/O_2=18$). The BCu3.72 sample contains crystalline CuO particles (PDF:45-0937) with 19±2 nm in size, while in the case of CuO/SiO_2 reference sample CuO peaks were also detected but the particle size was smaller, $d_{CuO}=13\pm1$ nm was determined. The low-loaded samples were not measured by XRD because of detection limit of the technique.

During TEM studies very few relatively large Cu containing particles were seen in BCu3.72 evidenced by EDS. In accordance with XRD results we suppose that they were CuO particles, however, the number of them was less than what 3.73 wt% CuO would present. Furthermore, EDS detected Cu signal at several places on the support together with Au signal, but there were places where Cu signal was not detected at all suggesting the inhomogeneous distribution of Cu in BCu3.72. At lower Cu-content (BCu1.04) EDS detected Cu signal at places, where Au particles were seen and on the bare silica as well. We must note, although, that the small contrast between SiO_2 and CuO does not allow one to easily spot copper oxide particles, if they are thin and small in size.

The Au particle sizes determined by TEM after catalytic run are around 6 nm except for the BCu1.04 ($d_{Au}=12.6nm$). The reason for this discrepancy will be clarified in the next future, whether it was caused by the presence of copper or an unexpected artefact happened during sol preparation or adsorption step of BCu1.04 (because it was prepared form another batch of Au sol than the others). The significantly lower standard deviations of average particle size of the BCu0.88Ce1.06 and ACu0.08 points to the importance of CeO_2 modifier introduced with method B and to the role

of small amount of copper, respectively, both acting as a kind of glue to prevent sintering during heat treatments.
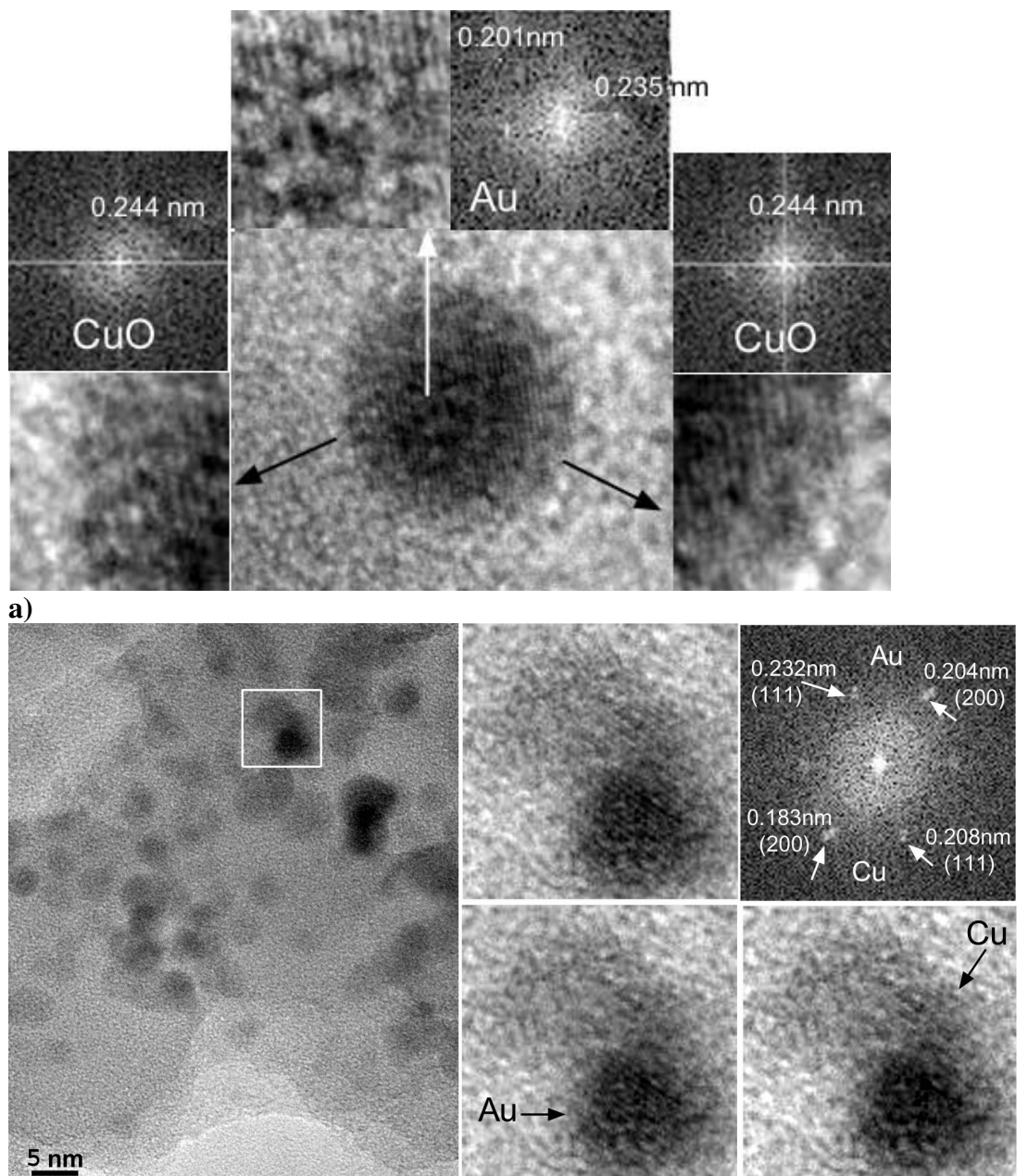
a)

b)

Figure 9 HRTEM image of BCu3.72 a) after calcination/450°C and catalytic run with CO/O$_2$=1/18 gas mixture; b) at the end of PROX measurements (for detailed conditions see the catalytic properties section, but shortly: calc+PROX+CO ox+red+PROX+CO ox)

HRTEM was applied to gain deeper insights into the location, size, and structure of the promoting oxide. Several samples were measured but it was very hard to find crystalline features other than gold nanoparticles. In the case of BCu3.72 after calcination treatment at 450°C CuO layers were detected around certain gold particles proving the existence of CuO decoration on gold (see Figure 9 a). Appearance of oxidic copper after calcination treatment is in accordance with the XRD results.

After reduction treatment followed by preferential CO oxidation reaction in the presence of large amount of hydrogen (see the next section) the reduction of oxide phase is expected to happen according to the TPR results (see above the TPR peak at ~ 260°C). Figure 9 b) shows that in

BCu3.72 metallic Cu particles are present separately and in close contact with Au particles. Beside Cu and Au particles, HRTEM gave a hint on the existence of AuCu particles as well.

In the case of method A, there is a slight chance for the formation of metallic Cu or Cu shell during preparation, since residual reducing agents (partially hydrolysed tannin and citrate) are still present in the Au sol. Literature reference revealed that pure Cu nanoparticles stabilized in water are sensitive to oxidation: they are stable under inert atmosphere but get oxidized on exposing to air[68]. We might assume the existence of metallic Cu around gold in the case of method A, just because of the presence of gold that can (partially) prevent reoxidation of reduced copper if any was formed. HRTEM investigation of calcined ACu0.08 detected lattice fringes that can be attributed to AuCu alloy phases and fringes that may present CuO, beside, obviously, lattice fringes of Au. After PROX measurements that include reduction of the sample, only Au and AuCu lattice parameters could be measured by HRTEM.

It seems that in the case of preparation method A there is a chance for the formation of bimetallic AuCu and CuO phase after calcination and CO oxidation. In the case of method B the identified phases are CuO, Au and some CuO can cover Au particles in the calcined sample. Reduction produces separate Cu particles at high Cu concentration (BCu3.72) and AuCu particles at very low Cu content (ACu0.08). However, we should keep in mind that inhomogeneous distribution of copper species was detected, thus fluctuation in composition and in arrangement of all phases present simultaneously in the sample is expected.

5.4. Catalytic properties

CO oxidation was used as a highly sensitive tool to test the influence of copper or copper oxide promoter on the activity of gold. The presence of Au-CuO(Cu) active interface was to be proven. The catalytic measurements were conducted after calcination treatments at 450°C which removed all carbonaceous deposits originated from the preparation. CO oxidation measurements were carried out in 3 different ways in a plug flow reactor: i) with 0.5% CO + 9% O_2 in He (CO/O_2=1/18), 30 mg sample, 55 ml/min flow rate, ii) with 1% CO + 1% O_2 in He (CO/O_2=1/1), 20 mg sample, 20 ml/min flow rate and iii) in presence of excess hydrogen with 1% CO + 1% O_2 + 60% H_2 // in He, 20 mg sample, 20 ml/min flow rate (PROX).

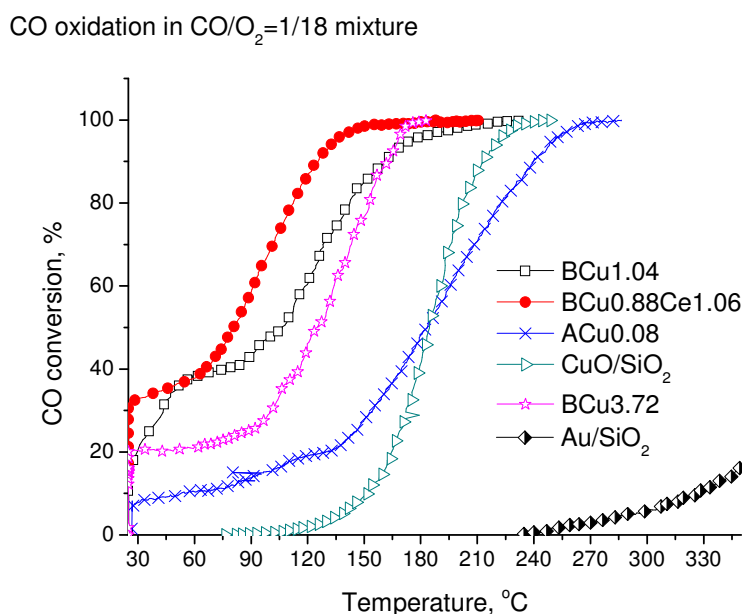Figure 10 shows the CO conversion curves obtained in the O_2 rich mixture (CO/O_2=18).

CO oxidation in CO/O_2=1/18 mixture

Figure 10 CO conversion curves obtained after calcination at 450°C using CO/O_2=1/18

It is clearly seen that all the samples possess some activity at room temperature except for the reference CuO/SiO_2 and Au/SiO_2. The best sample is the one containing CeO_2 beside Au and CuO and the least active one after calcination is ACu0.08. The less efficient catalytic behaviour of ACu0.08 among the Cu promoted samples might be explained by the least amount of copper oxide in contact with gold (based on the HRTEM results) or the most delicate way of decoration of Au(Cu) with oxidic copper. The active interface formed with ≥1wt% CuO and gold is obvious, since the activity of these samples are definitely higher than the sum of the activity of the reference Au/SiO_2 and the 4% CuO/SiO_2, although the structure of nanosize CuO must be different in each sample causing differences in activity.

The activity expressed as the temperature of 50% CO conversion versus CuO content is depicted in Figure 11. Very similar trend is seen like in the case of $Au-CeO_2-SiO_2$ system (see previous chapter) and the promoting influence of CeO_2 is also eye-catching.
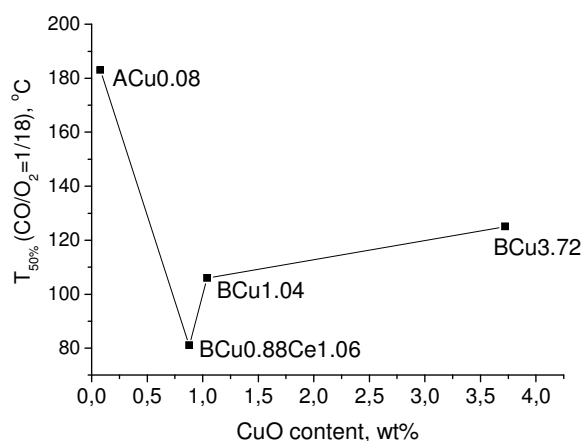

Figure 11 The temperature of 50% CO conversion versus CuO content using $CO/O_2=1/18$

The additional catalytic tests were conducted with less oxygen in the presence or in the absence of hydrogen, but with the same CO/O_2 ratio of 1/1. Measurements denoted as "PROX measurements" (for example in the discussion of HRTEM results) were carried out according to the following schedule:

1. calcination at $450^{o}C$ in air
2. temperature programmed (TP) PROX cycles with $CO/O_2/H_2 =1/1/60$ in He until stable performance
3. TP CO oxidation reactions with $CO/O_2=1/1$ in He until stable performance
4. reduction treatment at $450^{o}C$ in H_2
5. TP PROX cycles (heating and cooling curves) until stable performance
6. TP CO oxidation reactions with $CO/O_2=1/1$ until stable performance

PROX reaction after calcination treatment means the 2nd step in the above schedule, while *PROX reaction after reduction* refers to the 5th step and the same logic applies for the CO oxidations after calcination (3rd step) and after reduction (6th step) from now on.

Figure 12 compares the CO oxidation activities in the oxygen rich and lean mixtures. Activity is expressed in $T_{50\%}$. The main difference between the two oxidation reactions is that in the case of oxygen lean measurements the samples were contacted with 60% H_2 (in PROX reaction) prior to the simple CO oxidation reaction (data denoted as $T_{50\%}$ after calc+PROX) or were even reduced in pure hydrogen at $450^{o}C$ (data denoted as $T_{50\%}$ after red+PROX). This hydrogen atmosphere must have reduced most of the copper oxide, thus causing structural changes, although the particle size of gold did not change significantly as data in Table 3 shows.
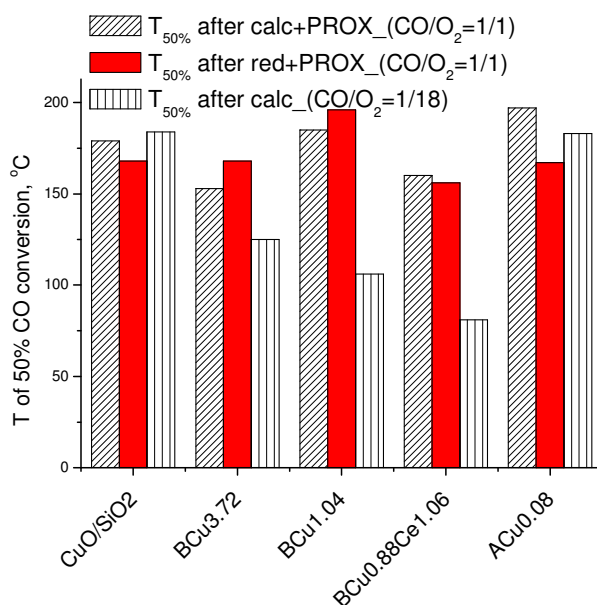
Figure 12 Comparison of CO oxidation activities in oxygen- lean and rich conditions

The activity order of the samples changes compared to the $CO/O_2=1/18$ case and the least difference is seen in the case of CuO/SiO_2 reference and ACu0.08 meaning that for these samples the least variation happens in the state of active sites upon reduction and decrease in O_2 concentration in the reactant mixture. On the contrary, the latter parameters seem to negatively influence the sample containing CeO_2 beside CuO. The data of Au/SiO_2 are not shown in Figure 12, because of its very low activity (in O_2 rich mixture it start to convert CO at ~230 °C, while in O_2 lean mixture maximum ~ 10% CO conversion is achieved under 100°C in both cases).
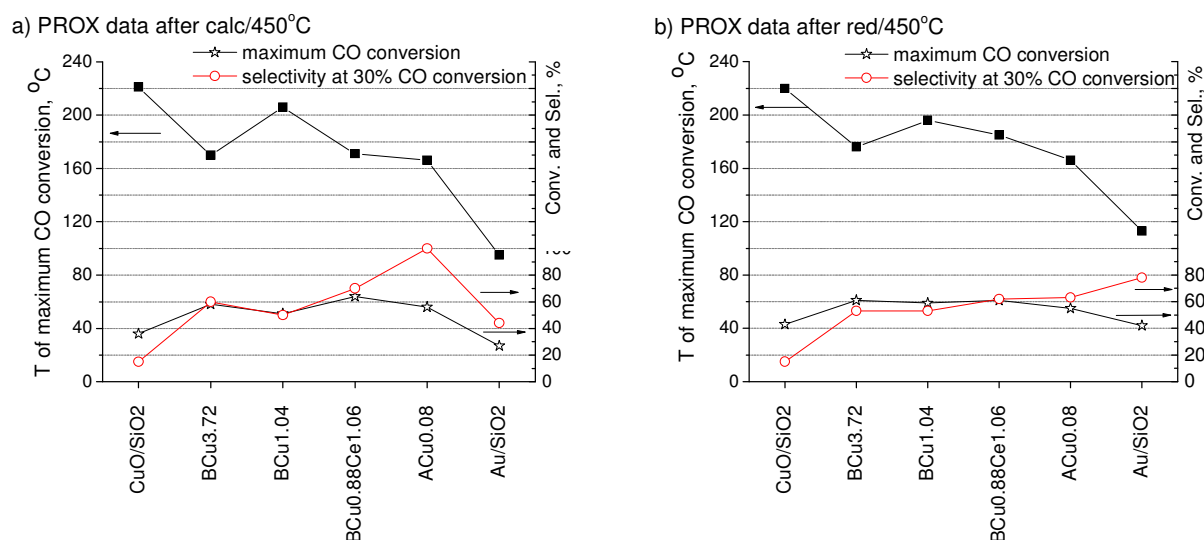

Figure 13 PROX data of the samples a) after calcination and b) after reduction

Let us consider now the PROX reaction itself. CO conversion goes through a maximum because at certain temperature the surface coverage of CO becomes so low that no longer poisons H_2 oxidation[63]. Selectivity is 100% if all the O_2 converted is used only for production of CO_2 and

not H_2O. We have to keep in mind that upon the contact with hydrogen (partial) reduction of copper oxide happens when increasing the temperature as above ~ $150^{o}C$ reduction of bulk CuO/SiO_2 starts (under the conditions of TPR). In Figure 13 a) and b) PROX evaluation is shown after the initial calcination and after the further reduction treatment, 2nd and 5th step in PROX measurements, respectively.

In the case of PROX after calcination (Figure 13 a) the temperature of maximum CO conversion increases for the Cu-containing samples and it is the highest for CuO/SiO_2 reference. Higher CO conversion was achieved with the samples containing Au and Cu compounds than with the reference samples. Concerning selectivities the apparent advantage of ACu0.08 above all other samples is obvious. Furthermore, the addition of CeO_2 modifier causes selectivity increase[69] among samples prepared by method B. Figure 13 b) shows basically the same trends but the differences between samples smoothen, the outstanding parameters of ACu0.08 vanish. This means reduction treatment at $450^{o}C$ forms very similar structures in AuCu-containing samples. The active sites are most probably AuCu and Au species in contact with thin metallic Cu or Cu^{+} particles, patches, and bulkier copper compounds which must exist at higher copper content do not contribute much to the activity.
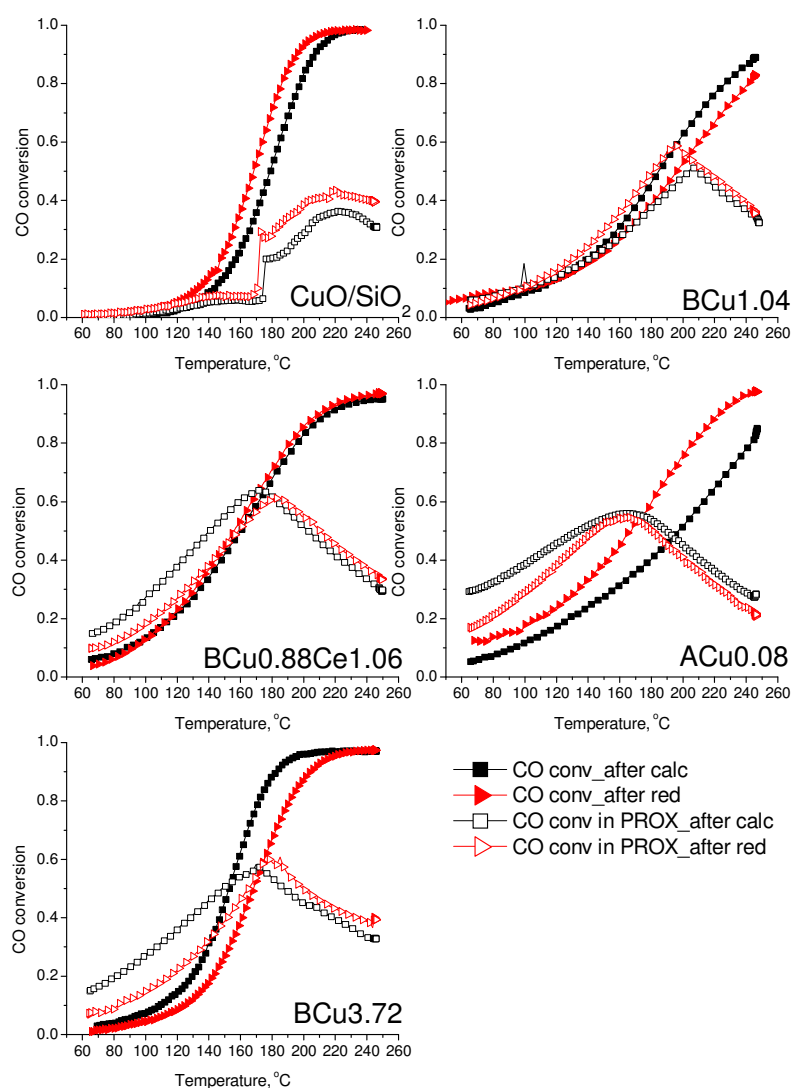

Figure 14 CO_2 conversion curves under PROX condition (in 60 % H_2) and without the presence of hydrogen using the same $CO/O_2=1/1$ ratio

Concluding all the PROX results, at lower temperature the reduced Au/SiO_2 catalyst is the best choice, while copper containing samples perform better above 100^oC. The superior PROX properties of AuCu(O) combination over pure Cu(CuO) is apparent at any conditions investigated. Structural investigations by XPS after in situ treatments will certainly provide deeper insights into the reasons of the above detailed catalytic behaviour via the clarification of oxidation states and surface concentration of copper species.

Finally an interesting comparison is depicted in Figure 14 which shows the CO_2 conversion curves under PROX condition (in $60\%H_2$) and without the presence of hydrogen using the same $CO/O_2=1/1$ ratio. There are several factors to correlate, but the most important observation is that the presence of hydrogen suppresses the conversion of CO only in the case of the reference CuO/SiO_2 suggesting that the adsorption and activation of CO molecules happens on the Au surface indeed in favour of that of hydrogen.

6. Other results obtained during our investigations

In addition to the research described above, which followed closely the research plan of the project, some other investigation were done, too, applying the advantages of the sol method in the controlled formation of gold based catalysts. Gold was modified with Pd fabricating bimetallic particles stabilised in aqueous sols by various ways (co- or subsequent reduction of precursor ions applying different reducing agents and stabilizers) resulting in different arrangement of the components in the nanoparticles, which deposited on a support were studied in CO oxidation[70] and acetylene hydrogenation[71]. Au supported on various oxide supports were compared in glucose selective oxidation and CO oxidation[72].

TiO_2 supported bimetallic Au–Pd catalysts were prepared by deposition of bimetallic aqueous sols formed (i) by co-reduction of the precursor ions by a mixture of Na-citrate and tannic acid, (ii) by reduction of Au in a preformed Pd sol and (iii) by reduction of Pd in a preformed Au sol. According to XRD studies all three samples contained a bimetallic phase of somewhat different composition. Both Au and Pd could be detected by XPS in the surface layers, but the Au/Pd ratio differed significantly in the three bimetallic samples. It was the largest in the sample, where the Au was reduced onto Pd sols, the lowest where the metal reduction was done in the reverse way, and intermediate for the Au/Pd co-reduced sample. The calcination/reduction treatment necessary for removal of organic residues did not affect the composition of the bimetallic crystalline phase, but it increased both the crystallite and particle sizes of the metals, and the calcination caused some Pd migration to the surface. The catalytic activity of the bimetallic samples regardless of the preparation method is about the same as that of the mixture of the Pd and Au monometallic samples. No significant synergism is suggested in the present bimetallic samples.

Au–Pd bimetallic particles were synthesized by reduction with 2-propanol and by pulse radiolysis technique. UV-Vis spectra measured as a function of time or pulse number confirm formation of Au_{core}–Pd_{shell} particles due to prevailing electron transfer between nascent Pd clusters and Au ions. It appears that the mode of reduction significantly affects the particle size: with the increase of the Au/Pd ratio the particle size steeply increased for the sols reduced with 2-propanol confirming the governing role of Pd in the reduction of Au^{3+} ions. Pulse radiolysis resulted in decreasing particle size for the Au rich particles due to fast reduction of Au^{3+} by solvated electrons. The Au/Pd bimetallic sols stabilized by PDDA polycation were adsorbed onto Aerosil SiO_2 by increasing the pH and thus increasing the negative charge on the silica surface. Gas phase hydrogenation of acetylene was tested at 45^oC on samples ''as received'', H_2 treated at 200^oC and O_2/H_2 treated at 250^oC. The hydrogenation activity of the ''as received'' samples proves that acetylene is able to find Pd sites on our PDDA stabilised surface. The O_2/H_2 treatment at 250^oC significantly enhanced the hydrogenation activity at the Pd rich compositions (10 and 20 at% Au) which observation can be attributed to the removal of PDDA from metallic sites and to intermixing of Au and Pd generating thereby gold diluted Pd–Au ensembles.

Two series of gold catalysts supported on SiO_2, CeO_2 and TiO_2 have been prepared by colloidal gold deposition method providing uniform original Au particles in the different catalysts favouring the investigation of support and size effect on CO oxidation and selective glucose oxidation catalytic activity. The diameter of gold particle stabilized by polyvinylalcohol (PVA) or by tannic acid-citrate was 2–3 nm and 6–7 nm, which increased to 5–7 nm and 7–13 nm, respectively, after calcination in air. Inverse correlation was found between the activities in CO and glucose oxidation (the silica supported, larger size Au particles were more active in glucose and less active in CO oxidation) suggesting that the mechanisms are different which is explained by geometrical and support effects. The results show that the effect of the support is more significant than the small gold particle size. (The product analysis of the glucose oxidation reaction was performed by the HPLC instrument purchased by the financial support of several OTKA grants including the present one.)

7. Final evaluation of the different systems

During the research work reported here Au/SiO_2 catalysts promoted by "active oxides" such as TiO_2, CeO_2, CuO were developed and investigated for catalytic purposes. These so-called inverse catalysts, when Au is decorated by moieties of the active oxide, were produced using two parallel methods based on the application of Au sols. The Au sol was produced by tannin/citrate reduction and contained Au nanoparticles of about 6 nm, while precursors of TiO_2, CeO_2 and CuO promoters were Ti(IV)-lactate complex, Ce(III) nitrate and Cu(II) nitrate, respectively. The Au content was kept constants in the SiO_2 supported samples while the loading of active oxide was varied. In method A, the precursor of promoter was added to the Au sol and after a heat treatment at $60^{o}C$ the adsorption step onto SiO_2 was accomplished using PDDA polycation. In method B, the precursor of promoter was added to the washed and dried Au/SiO_2 parent catalyst producing a suspension which was kept also at $60^{o}C$ until the evaporation of water. All samples were calcined before use to remove organic deposits and convert all promoter species into oxide form.

The success of our approach, namely, the localized oxide promotion of gold on silica was ascertained by structural investigations (TEM, HRTEM, XRD, TPR) and catalytic tests in CO oxidation in the presence and absence of hydrogen. The main general conclusions regarding all the systems are as follows:

- The stabilization of Au particle size could be achieved by the controlled addition of promoter oxides compared to the case, when Au is supported on pure/bulk active oxide.
- Using method A the decoration of Au with nanosize promoter oxide particles, patches happens at very low TiO_2, CeO_2, CuO content. Depending on the nature of oxide precursor, increasing the precursor concentration higher loading can also be achieved, but in this case above a given concentration the promoter oxide covers in increasing extent the pure SiO_2 surface, as well. Ti species originating form Ti-lactate complex favour the additional deposition on silica, copper species only partially, while ceria precursor species do not tend to be bound to the positively charged silica surface. The local enrichment of active oxide on gold nanoparticles is suggested to happen in the case of method B as well, although to a different extent.
- The above mentioned decoration of Au particles by the promoters is governed by the attraction of stabilizing sphere around Au nanoparticles composed of tannin/citrate moieties, which still exists also in supported form after washing and drying. Electrostatic interactions and complex formation between the organic shell and the active oxide precursors, which might be partially hydrolyzed, are suggested to prevail. Furthermore, the PDDA polycation assisted attachment of sol components plays a crucial role in preparing the supported samples.
- Catalytic activity of the nanostuctured Au-active oxide ensemble on SiO_2 is much higher than that of the reference samples, when Au particles with the same or similar size are supported on bulk active oxides. The best catalytic performance is achieved at different oxide loadings

depending on the type of promoter. The most dramatic activity increase and so the most intriguing effect of nanosize oxide decoration on Au was observed in the case of CeO_2 – modifications, when 0.16wt% CeO_2 was enough to approach closely the activity of the Au/CeO_2 reference sample. The promoter oxide-Au interface in contact with SiO_2 underneath behaves in a synergetic way and may provide more active oxygen to the reaction and may also affect the adsorption of reactant molecules via special electronic interactions.

- CO oxidation in the presence of hydrogen (PROX) carried out on CuO-modified samples suggested that depending on the preparation method, metal loading and reaction condition, the oxidation state of copper species during the catalytic reaction can be varied.

- Comparing the systems investigated, the most efficient catalysts in CO oxidation are the CeO_2-containing samples followed by TiO_2 and than CuO_x-containing ones. In PROX process the CeO_2- and CuO_x-modified catalysts provided higher maximum CO conversion (around 60-70% and 50-60% at about 140-160 and 160-180°C, respectively) than the TiO_2-modified ones (<40% maximum CO conversion at about 80-100°C).

References

1   G. C. Bond, C. Louis, D. T. Thompson: Catalysis by Gold (Catalytic Science Series - Vol.6, series editor: G. J. Hutchings) Imperial College Press, 2006
2   M. J. Lippits, A. C. Gluhoi, B. E. Nieuwenhuys, Top. Catal. 44 (2007) 159-165
3   C. J. Weststrate, A. Resta, R. Westerström, E. Lundgren, A. Mikkelsen, J. N. Andersen, J. Phys. Chem. C 112 (2008) 6900-6906
4   M. P. Casaletto, A. Longo, A. M. Venezia, A. Martorana, A. Prestianni, Appl. Catal. A: Gen. 302 (2006) 309-316
5   M. Han, X. Wang, Y. Shen, Ch. Tang, G. Li, R. Smith, J. Phys. Chem. C 114 (2010) 793-798
6   F. Vindingi, M. Manzoli, A. Chiorino, F. Boccuzzi, Gold Bull. 42 (2009) 106-112
7   R. Grisel, K.-J. Westrate, A. Gluhoi, B. E. Nieuwenuys, Gold Bull. 35 (2002) 39-45
8   M. M. Schubert, S. Hackenberg, A. C. van Veen, M. Muhler, V. Plzak,R. J. Behm, J. Catal. 197 (2001) 113-122
9   L. Guczi, G. Pető, A. Beck, K. Frey, O. Geszti, Gy. Molnár, Cs. Daróczi, J. Am. Chem. Soc. 125 (2003) 4332-4337
10 L. Guczi, K. Frey, A. Beck, G. Pető, Cs. Daróczi, N. Kruse, S. Chenakin, Appl. Catal. A: Gen. 291 (2005) 116-125
11 K. Frey, A. Beck, G. Petõ, Gy. Molnár, O. Geszti, L. Guczi, Cat. Comm. 7 (2005) 64-67
12 L. Guczi, A. Beck, A. Horváth, Zs. Koppány, G. Stefler, K. Frey, I. Sajo, O. Geszti, D. Bazin, J. Lynch, J. Mol. Cat. (2003) 545-552
13 A.M. Venezia, F. L. Liotta, G. Pantaleo, A. Beck, A. Horváth, O. Geszti, A. Kocsonya, L. Guczi, Appl. Catal. A: Gen. 310 (2006) 114-121
14 A. Horváth, A. Beck, A. Sárkány, Gy. Stefler, Zs. Varga. O. Geszti, L. Tóth, L. Guczi, J. Phys. Chem. B 110 (2006) 15417-15425
15 C. Wang, C. Liu, J. Chen, T. Shen, J. Coll. Int. Sci. 191 (1997) 464-470
16 S. Zhao, S. Chen, S. Wang, Z. Quan, J. Coll. Int. Sci. 221 (2000) 161-165
17 V. Subramanian, E. E. Wolf, P. V. Kamat, J. Am. Chem. Soc. 126 (2004) 4943-4950
18 C. Wang, C. Liu, X. Zheng, J. Chen, . Shen, Coll. Surf. A: Physicochemical and Eng. Aspects 131 (1998) 271-280
19 M. Anija, J. Thomas, N. Singh, A. S. Nair, R. T. Tom, T. Padeep, R. Philip, Chem. Phys. Lett.380 (2003) 223-229
20 R. T. Tom, A. S. Nair, N. Singh, M. Aslam, C. L. Nagendra, R. Philip, K. Vijayamohanan, T. Pradeep, Langmuir 19 (2003) 3439-3445
21 A. Beck, A. Horváth, G. Stefler, M. S. Scurrell, L. Guczi, Top. Catal. 52 (2009) 912-919
22 M. Lütt, M. R. Fitzsimmons, D. Li, J. Phys. Chem. B 102 (1998) 400-405
23 H. Hattori, Thin Solid Films 385 (2001) 302-306
24 K. Ariga, Y. Lvov, I. Ichinose, T. Kunitake, Appl. Clay Sci. 15 (1999) 137-152
25 A. Horváth, A. Beck, A. Sárkány, L. Guczi, J. Mol. Catal. A: Chemical, 182-183 (2002) 295-302
26 H. Möckel, M. Giersig, F. Willig, J. Mater. Chem., 9 (1999) 3051-3056
27 J. Duan, J. Gregory, Adv. Coll. Int. Sci. 100-102 (2003) 474-502
28 Z. Su, X. Chang, G. Zhan, X. Luo, Q. Pu, Analytica Chimica Acta 310 (1995) 493-499
29 L. Xue, Q. Li, Y. Zhang. R. Liu, X. Z. Hen, J. Eur. Cer. Soc. 26 (2006) 323-329
30 X. Shi, T.. Cassagneau, F. Caruso, Langmuir 18 (2002) 904-910
31 Y.-G. Guo, L.-J. Wan, C.-L. Bai, J. Phys. Chem. B 107 (2003) 5441-5444
32 T. Shutava, M. Prouty, D. Kommireddy, Y. Lvov, Macromlolecules 38 (2005) 2850-2858

33 Y. Miyazaki, S. Shiratori, Thin Solid Films 499 (2006) 29-34

34 Y. Tai, J. Murakami, K. Tajiri, F. Ohashi, M. Daté, S. Tsubota, Appl. Catal. A: Gen. 268 (2004)183-187

35 M. Olea, Y. Iwasawa, Applied. Catal. A: Gen. 275 (2004) 35-42

36 H. Liu, A. I. Kozlov, A. P. Kozlova, T. Shido, K. Asakura, Y. Iwasawa, J. Catal. 185 (1999) 252-264

37 L. Guczi, A. Beck, A. Horváth, A. Sárkány, Gy. Stefler, O. Geszti, Stud. Surf. Sci. Catal. 172 (2007) 221-224

38 A. Beck, A. Horváth, Gy. Stefler, R. Katona, O. Geszti, Gy. Tolnai, L. F. Liotta, L. Guczi, Catal. Today 139 (2008) 180-187

39 G. Yi, Z. Xu, G. Guo, K. Tanaka, Y. Yuan, Chem. Phys. Lett. 479 (2009) 128-132

40 L. Escamilla-Perea, R. Nava, B. Pawelec, M. G. Rosmaninho, C. L. Peza-ledesma, J. L. G. Fierro, Appl. Catal. A: Gen. 381 (2010) 42-53

41 K. Qian, S. Lv, X. Xiao, H. Sun, J. Lu, M. Luo, W. Huang, J. Mol. Cat. A : Chem. 306 (2009) 40-47

42 P. Castano, T. A. Zepeda, B. Pawelec, M. Makkee, J. L. G. Fierro, J. Catal. 267 (2009) 30-39

43 J. A. Hernandez, S. Gómez, B. Pawelec, T. A. Zepeda, Appl. Catal. B: Environmental 89 (2009) 128-136

44   S. D. Senanayake, D. Stacchiola, J. Evans, M. Estrella, L. Barrio, M. Pérez, J. Hrbek, J. A. Rodriguez, J. Cat. 271 (2010) 392-400

45 C. M. Y. Yeung, S. C. Tsang, J. Mol. Cat. A: Chem. 322 (2010) 17-25

46 Q. Yuan, H.-H. Duan, L.-L. Li, L.-D. Sun, Y.-W. Zhang, C.-H. Yan, J. Coll. Int. Sci. 335 (2009) 151-167

47 M-H. Oh, J-S. Nho, S-B. Cho, J-S. Lee, R. K. Singh, Materials Chem. Phys. 124 (2010) 134-139

48 A. A. Athawale, M. S. Bapat, P. A. Desai, J. Alloys and Compounds 484 (2009) 211-217

49 T. S. Anirudhan, P. S. Suchithra, Appl. Clay Sci. 42 (2008) 214-223

50 A. Ohyoshi, E. Ohyoshi, H. Ono, S. Yamanaka, J. Inorg. Nucl. Chem. 34 (1972) 1955-1960

51 N. A. Oladoja, Y. B. Alliu, A. E. Ofomaja, I. E. Unuabonah, Desalination 271 (2011) 34-40

52 H. Holness, Anal. Chim. Acta 3 (1949) 290-294

53 A. Horváth, A. Beck, Gy. Stefler, T. Benkó, Gy. Sáfrán, Zs. Varga, J. Gubicza, L. Guczi, J,. Phys. Chem. C, submitted

54 G. Avgouropoulos, T. Ioannides, Ch. Papadopoulou, J. Batista, S. Hocevar, H. K. Matralis, Catal. Today, 75 (2002) 157-167

55 R. Lin, M.-F. Luo, Y.-J. Zhong, Z.-L. Yan,, G.-Y. Liu, W.-P. Liu, Appl. Catal. A: Gen. 255 (2003) 331-336

56 X. Tang, B. Zhang, Y. Li, Y. Li, Y. Xu, Q. Xin, W. Shen, Catal. Today 93-95 (2004) 191-198

57 C. R. Jung, J. Han, S. W. Nam, T.-H. Lim, S.-A. Hong, H.-I. Lee, Catal. Today 93-95 (2004) 183-190

58 Y. Liu, Q. Fu, M. F. Stephanopoulos, Catal. Today 93-95 (2004) 241-246

59 R. J. H. Grisel, B. E. Nieuwenhuys, Catal. Today 64 (2001) 69-81

60 A. C. Gluhoi, N. Bogdanchikova, B. E. Nieuwenhuys, Catal. Today 113 (2006) 178-181

61 X. Liu, A. Wang, T. Zhang, D.-S. Su, C.-Y. Mou, Catal. Today, 160 (2011) 103-108

62 X. Liu, A. Wang, L. Li, T. Zhang, C.-Y. Mou, J.-F. Lee J. Catal. (2011), doi:10.1016/j.jcat.2010.12.016

63 T. S. Mozer, D. A. Dziuba, C. T. P. Vieira, F. B. Passos, J. Power Sources 187 (2009) 209-215

64 R. J. Chimentao, F. Medina, J. L. G. Fierro, J. Llorca, J. E. Sueiras, Y. Cesteros, P. Salagre, J. Mol. Cat. A: Chem. 274 (2007) 159-168

65 J. Llorca, M. Domínguez, C. Ledesma, R. J. Chimentao, F. Medina, J. Sueiras, I. Angurell, M. Seco, O. Rossell, J. Catal. 258 (2008) 187-198

66 E. Beltowska-Lehman, Surf. Coat. Techn. 151-152 (2002) 440-443

67 S. H. Y. Lo, Y.-Y. Wang, C.-C. Wan, J. Coll. Int. Sci. 310 (2007) 190-195

69 G. Avgouropoulos, T. Ioannides, Appl. Catal. B: Environmental 67 (2006) 1-11

70 A. Beck, A. Horváth, Z. Schay, Gy. Stefler, Zs. Koppány, I. Sajó, O. Geszti, L. Guczi, Topics in Catalysis 44 (2007) 115-121

71 A. Sárkány, P. Hargitai, A. Horváth, Topics in Catalysis 46 (2007) 121-128

72 T. Benkó, A. Beck, O. Geszti, R. Katona, A. Tungler, K. Frey, L. Guczi, Z. Schay, App. Cat. A 388 (2010) 31-36